PHYSICAL REVIEW D **79,** 014013 (2009)

$B \to S$ transition form factors in the perturbative QCD approach

Run-Hui Li,[1,2] Cai-Dian Lü,[2,3] Wei Wang,[2] and Xiao-Xia Wang[2]

[1]*School of Physics, Shandong University, Jinan, Shandong 250100, China*

[2]*Institute of High Energy Physics, P.O. Box 918(4), Beijing 100049, China*

[3]*Department of Physics and Institute of Theoretical Physics, Nanjing Normal University, Nanjing 210097, China*

(Received 21 November 2008; published 20 January 2009)

Under two different scenarios for the light scalar mesons, we investigate the transition form factors of $B(B_s)$ mesons decay into a scalar meson in the perturbative QCD approach. In the large recoiling region, the form factors are dominated by the short-distance dynamics and can be calculated using perturbation theory. We adopt the dipole parametrization to recast the q^2 dependence of the form factors. Since the decay constants defined by the scalar current are large, our predictions on the $B \to S$ form factors are much larger than the $B \to P$ transitions, especially in the second scenario. Contributions from various light-cone distribution amplitudes (LCDAs) are elaborated and we find that the twist-3 LCDAs provide more than one-half of the contributions to the form factors. The two terms of the twist-2 LCDAs give destructive contributions in the first scenario while they give constructive contributions in the second scenario. With the form factors, we also predict the decay width and branching ratios of the semileptonic $B \to Sl\bar{\nu}$ and $B \to Sl^+l^-$ decays. The branching ratios of $B \to Sl\bar{\nu}$ channels are found to have the order of 10^{-4} while those of $B \to Sl^+l^-$ have the order of 10^{-7}. These predictions can be tested by the future experiments.

DOI: 10.1103/PhysRevD.79.014013 PACS numbers: 13.25.Hw

I. INTRODUCTION

Although a number of scalar states have been discovered long time ago, the underlying structure of scalar mesons has not been well established (for a review, see [1–3]). In order to uncover the inner structures, many different descriptions have been proposed such as $\bar{q}q$, $\bar{q}\,\bar{q}\,qq$, meson-meson bound states, or even supplemented with a scalar glueball. It is very likely that they are not made of one simple component but are the superpositions of these contents. The different scenarios tend to give very different predictions on the production and decay of the scalar mesons which are helpful to determine the dominant component. Although intensive study has been given to the decay property of the scalar mesons, the production of these mesons can provide a different unique insight to the mysterious structure of these mesons, especially their production in B decays.

In B meson decays, the energy release is much larger and many channels involving a scalar meson in the final state are open. Since the first observation of the scalar meson $f_0(980)$ in three-body B meson decays $B^- \to K^- f_0(980) \to K^-(\pi^+\pi^-)$ [4], the two collaborations, *BABAR* and Belle, have reported many studies on decays involving a scalar meson in the final state: the branching ratios and/or direct CP asymmetries are measured or set an upper limit [5]. Since much more interesting channels are still not observed at present, it is just the beginning of scalar meson study in B factories. Meanwhile, it is also necessary to provide more theoretical studies which are useful for future experiments.

Theoretically, the studies on hadronic B decays are usually polluted by the nonperturbative QCD effect and predictions on the observables always suffer large uncertainties. Since there is only one hadron in the final state in semileptonic $B \to S$ decays, they receive less theoretical uncertainties. In these channels, the most challenging part in the calculation is the matrix element of the $B_{(s)}$ to scalar meson transition. In the region of small recoil, where q^2 is large, the form factors are dominated by the soft dynamics, which is out of control of perturbative QCD. However, in the large-recoil region where $q^2 \to 0$, roughly 5 GeV of energy is released. About half of this energy is taken by the light scalar meson, which suggests that large momentum is transferred in this process and the interaction is mainly dominated by the short-distance dynamics. Therefore the perturbative QCD approach (pQCD) [6] is expected to be applicable to B to scalar meson transitions in the large-recoil region. With the results obtained in the restricted region, one can extrapolate these form factors to the whole kinematic region by adopting some parametrization form for the form factors.

This paper is organized as follows: The distribution amplitudes and decay constants of the mesons are given in Sec. II. In Sec. III we listed the formulas about the form factors and semileptonic decays. Section IV is a discussion of the numerical results. The Appendix lists the useful functions for the pQCD approach.

II. CONVENTIONS AND INPUTS

We will work in the rest frame of the B meson and use the light-cone coordinates. In the heavy quark limit the mass difference of b quark and B meson is negligible: $m_b \simeq m_B$. The masses of scalar mesons are very small compared with the b quark mass, we keep them up to the

first order. Since the scalar meson in the final state moves very fast in the large-recoil region, we define the momentum of the scalar meson on the plus direction in the light-cone coordinates. The momentum of the B meson and scalar mesons can be denoted as

$$P_B = \frac{m_B}{\sqrt{2}}(1, 1, 0_\perp), \qquad P_S = \frac{m_B}{\sqrt{2}}(\eta, 0, 0_\perp). \tag{1}$$

Then for momentum $q = P_B - P_S$, there exists $\eta = 1 - q^2/m_B^2$. The momentum of the light antiquark in B meson and the quark in scalar mesons are denoted as k_1 and k_2 respectively (see Fig. 1):

$$k_1 = \left(0, \frac{m_B}{\sqrt{2}}x_1, \mathbf{k}_{1\perp}\right), \qquad k_2 = \left(\frac{m_B}{\sqrt{2}}x_2\eta, 0, \mathbf{k}_{2\perp}\right). \tag{2}$$

In the course of the pQCD calculations, the light-cone wave functions of the mesons are required. The B meson is a heavy-light system, and its light-cone matrix element can be decomposed as [7]

$$\begin{aligned}\int_0^1 \frac{d^4z}{(2\pi)^4} e^{ik_1\cdot z}\langle 0|b_\beta(0)\bar{q}_\alpha(z)|\bar{B}_{(s)}(P_{B_{(s)}})\rangle \\ = \frac{i}{\sqrt{2N_c}}\Big\{(\not{P}_{B_{(s)}} + m_{B_{(s)}})\gamma_5\Big[\phi_{B_{(s)}}(k_1) \\ + \frac{\not{n} - \not{v}}{\sqrt{2}}\bar{\phi}_{B_{(s)}}(k_1)\Big]\Big\}_{\beta\alpha},\end{aligned} \tag{3}$$

where $n = (1, 0, \mathbf{0}_T)$ and $v = (0, 1, \mathbf{0}_T)$ are lightlike unit vectors. There are two Lorentz structures in B meson light-cone distribution amplitudes, and they obey the normalization conditions:

$$\int \frac{d^4k_1}{(2\pi)^4}\phi_{B_{(s)}}(k_1) = \frac{f_{B_{(s)}}}{2\sqrt{2N_c}}, \qquad \int \frac{d^4k_1}{(2\pi)^4}\bar{\phi}_{B_{(s)}}(k_1) = 0, \tag{4}$$

with $f_{B_{(s)}}$ as the decay constant of the $B_{(s)}$ meson. In principle, both the $\phi_{B_{(s)}}(k_1)$ and $\bar{\phi}_{B_{(s)}}(k_1)$ contribute in B meson transitions. However, the contribution of $\bar{\phi}_{B_{(s)}}(k_1)$ is usually neglected, because its contribution is numerically small [8]. So we will only keep the term with $\phi_{B_{(s)}}(k_1)$ in Eq. (3). In the momentum space the light-cone matrix of B meson can be expressed as

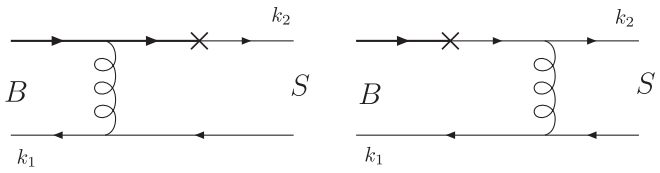

FIG. 1. Contributions to the form factors in the pQCD approach, where the cross denotes the weak vertex.

$$\Phi_{B_{(s)}} = \frac{i}{\sqrt{6}}(\not{P}_{B_{(s)}} + m_{B_{(s)}})\gamma_5\phi_{B_{(s)}}(k_1). \tag{5}$$

Usually the hard part is independent of k^+ or/and k^-, so we integrate one of them out from $\phi_{B_{(s)}}(k^+, k^-, \mathbf{k}_\perp)$. With b as the conjugate space coordinate of $\mathbf{k}_\perp$, we can express $\phi_{B_{(s)}}(x, \mathbf{k}_\perp)$ in b space by

$$\Phi_{B_{(s)},\alpha\beta}(x, b) = \frac{i}{\sqrt{2N_c}}[\not{P}_{B_{(s)}}\gamma_5 + m_{B_{(s)}}\gamma_5]_{\alpha\beta}\phi_{B_{(s)}}(x, b), \tag{6}$$

where x is the momentum fraction of the light quark in the B meson. In this paper, we use the following expression for $\phi_{B_{(s)}}(x, b)$:

$$\phi_{B_{(s)}}(x, b) = N_{B_{(s)}}x^2(1 - x)^2\exp\left[-\frac{m_{B_{(s)}}^2x^2}{2\omega_b^2} - \frac{1}{2}(\omega_b b)^2\right], \tag{7}$$

with $N_{B_{(s)}}$ is the normalization factor, which is determined by Eq. (4). In recent years, a lot of studies for $B^\pm$ and B_d^0 decays have been performed by the pQCD approach [6]. With the rich experimental data, the ω_b in (7) is fixed as 0.40 GeV. In our calculation, we adopt $\omega_b = (0.40 \pm 0.05)$ GeV and $f_B = (0.19 \pm 0.025$ GeV) for B mesons. For the B_s meson, taking the SU(3) breaking effects into consideration, we adopt $\omega_{b_s} = (0.50 \pm 0.05)$ GeV and $f_{B_s} = 0.23 \pm 0.03$ GeV [9].

In the spectroscopy study, many scalar states have been discovered. Among them, the scalar mesons below 1 GeV, including $f_0(600)(\sigma)$, $f_0(980)$, $K_0^*(800)(\kappa)$, and $a_0(980)$, are usually viewed to form an SU(3) nonet; while scalar mesons around 1.5 GeV, including $f_0(1370)$, $f_0(1500)/f_0(1700)$, $K_0^*(1430)$, and $a_0(1450)$, form another nonet. There are two different scenarios to describe these mesons in the quark model. The first one (called scenario 1 in this paper) is the naive 2-quark model: the nonet mesons below 1 GeV are treated as the lowest lying states, and the ones near 1.5 GeV are the first excited state. In this scenario, the flavor wave functions of the light scalar mesons are

$$\begin{aligned}&\sigma = \frac{1}{\sqrt{2}}(u\bar{u} + d\bar{d}), \qquad f_0 = s\bar{s}, \qquad a_0^+ = u\bar{d}, \\ &a_0^0 = \frac{1}{\sqrt{2}}(u\bar{u} + d\bar{d}), \qquad a_0^- = d\bar{u}, \qquad \kappa^+ = u\bar{s}, \\ &\kappa^0 = d\bar{s}, \qquad \bar{\kappa}^0 = s\bar{d}, \qquad \kappa^- = s\bar{u}.\end{aligned} \tag{8}$$

Here it is supposed that the σ and $f_0(980)$ have the ideal mixing. However, the data of J/ψ decays does not favor $f_0(980)$ as a pure $s\bar{s}$ state [10], and it seems that σ and $f_0(980)$ have a mixing like

$$|f_0(980)\rangle = |s\bar{s}\rangle\cos\theta + |n\bar{n}\rangle\sin\theta,$$
$$|\sigma\rangle = -|s\bar{s}\rangle\sin\theta + |n\bar{n}\rangle\cos\theta, \tag{9}$$

with $|n\bar{n}\rangle = \frac{1}{\sqrt{2}}(u\bar{u} + d\bar{d})$ and θ as the mixing angle. The above description has encountered several severe difficulties. For example, if the $\bar{q}q$ states have the quantum numbers $J^{PC} = 0^{++}$, the corresponding masses are expected larger than that of the vector mesons. Studies on the mixing angle of σ and $f_0(980)$ [11] show that θ tends to be not a unique value, which indicates that σ and $f_0(980)$ may not be purely $q\bar{q}$ states. Based on these facts, the second scenario is proposed, where the nonet mesons near 1.5 GeV are viewed as the lowest lying states, while the mesons below 1 GeV may be viewed as four-quark bound states. Because of the difficulty when dealing with four-quark states, we only do the calculation about the heavier nonet in this scenario.

The decay constants of scalar mesons are defined by [10]

$$\langle S(p)|\bar{q}_2\gamma_\mu q_1|0\rangle = f_S p_\mu, \qquad \langle S|\bar{q}_2 q_1|0\rangle = m_S\bar{f}_S. \tag{10}$$

Because of the charge conjugate invariance, neutral scalar mesons cannot be produced by the vector current and thus

$$f_\sigma = f_{f_0} = f_{a_0^0} = 0. \tag{11}$$

For other scalar mesons, the vector decay constant f_S and scalar decay constant $\bar{f}_S$ (listed in Table I and II) is related by equations of motion $\mu_s f_S = \bar{f}_S$, with $\mu_s = \frac{m_S}{m_2(\mu)-m_1(\mu)}$. m_S is the mass of the scalar meson, and m_1, m_2 are the running current quark masses. All the inputs of the scalar mesons in our calculation, including the decay constants, running quark masses and the Gegenbauer moments, are quoted from [10].

The definition of twist-2 light-cone distribution amplitude (LCDA) $\Phi_S(x)$ and twist-3 LCDAs $\Phi_S^s(x)$ and Φ_S^σ for the scalar mesons can be combined into a single matrix element [10]:

TABLE I. Decay constants $\bar{f}_S$ (in units of MeV) and Gegenbauer moments at scale $\mu = 1$ GeV in scenario 1.

	$\bar{f}_S$	B_1	B_3
$a_0(980)$	365 ± 20	-0.93 ± 0.10	0.14 ± 0.08
$a_0(1450)$	-280 ± 30	0.89 ± 0.20	-1.38 ± 0.18
$f_0(980)$	370 ± 20	-0.78 ± 0.08	0.02 ± 0.07
$f_0(1500)$	-255 ± 30	0.80 ± 0.40	-1.32 ± 0.14
$\kappa(800)$	340 ± 20	-0.92 ± 0.11	0.15 ± 0.09
$K_0^*(1430)$	-300 ± 30	0.58 ± 0.07	-1.20 ± 0.08

TABLE II. Decay constants $\bar{f}_S$ (in units of MeV) and Gegenbauer moments at scale $\mu = 1$ GeV in scenario 2.

	$\bar{f}_S$	B_1	B_3
$a_0(1450)$	460 ± 50	-0.58 ± 0.12	-0.49 ± 0.15
$f_0(1500)$	490 ± 50	-0.48 ± 0.11	-0.37 ± 0.20
$K_0^*(1430)$	445 ± 50	-0.57 ± 0.13	-0.42 ± 0.22

$$\begin{aligned}\langle S(P_S)|q(0)_j\bar{q}(z)_l|0\rangle &= \frac{-1}{\sqrt{2N_c}}\int_0^1 dx e^{ixp\cdot z}\Big\{\not{p}_S\Phi_S(x) \\ &\quad + m_S\Phi_S^s(x) + m_S\sigma_{\mu\nu}P_S^\mu z^\nu\frac{\Phi_S^\sigma(x)}{6}\Big\}_{jl} \\ &= \frac{-1}{\sqrt{2N_c}}\int_0^1 dx e^{ixp\cdot z}\{\not{p}_S\Phi_S(x) \\ &\quad + m_S\Phi_S^s(x) + m_S(\not{n}\not{v} - 1)\Phi_S^T(x)\}_{jl},\end{aligned} \tag{12}$$

with the normalization conditions

$$\begin{aligned}\int_0^1 dx\phi_S(x) &= \frac{f_S}{2\sqrt{2N_c}}, \\ \int_0^1 dx\phi_S^s(x) &= \int_0^1 dx\phi_S^\sigma(x) = \frac{\bar{f}_S}{2\sqrt{2N_c}}.\end{aligned} \tag{13}$$

The LCDAs can be expanded in Gegenbauer polynomials as the following form:

$$\begin{aligned}\phi_S(x) &= \frac{f_S}{2\sqrt{2N_c}}6x(1-x)\Big[1 + \mu_s\sum_{m=1}^{\infty}B_m(\mu) \\ &\quad \times C_m^{3/2}(2x-1)\Big] \\ &= \frac{\bar{f}_S}{2\sqrt{2N_c}}6x(1-x)\Big[\frac{1}{\mu_s} + \sum_{m=1}^{\infty}B_m(\mu) \\ &\quad \times C_m^{3/2}(2x-1)\Big],\end{aligned} \tag{14}$$

$$\phi_S^s(x) = \frac{\bar{f}_S}{2\sqrt{2N_c}}\Big[1 + \sum_{m=1}^{\infty}a_m(\mu)C_m^{1/2}(2x-1)\Big], \tag{15}$$

$$\begin{aligned}\phi_S^T(x) &= \frac{d}{dx}\frac{\phi_S^\sigma(x)}{6} \\ &= \frac{\bar{f}_S}{2\sqrt{2N_c}}\frac{d}{dx}\Big\{x(1-x) \\ &\quad \times\Big[1 + \sum_{m=1}^{\infty}b_m(\mu)C_m^{3/2}(2x-1)\Big]\Big\},\end{aligned} \tag{16}$$

where $B_m(\mu)$, $a_m(\mu)$, and $b_m(\mu)$ are the Gegenbauer moments and $C_m^{(3/2)}$ and $C_m^{1/2}$ are the Gegenbauer polynomials. The values of $B_m(\mu)$ are listed in Tables I and II. And the values of $b_m\mu$ and $a_m(\mu)$ in scenario 2 are worked out in [12], which is listed in Table III. However, in the calcu-

TABLE III. Gegenbauer moments for the twist-3 LCDAs of scalar mesons at the scale $\mu = 1$ GeV in scenario 2 [12].

State	$a_1(\times 10^{-2})$	a_2	a_4	$b_1(\times 10^{-2})$	b_2	b_4
$a_0(1450)$	0	$-0.33 \sim -0.18$	$-0.11 \sim 0.39$	0	$0 \sim 0.058$	$0.070 \sim 0.20$
$K_0^*(1430)$	$1.8 \sim 4.2$	$-0.33 \sim -0.025$	$\cdots$	$3.7 \sim 5.5$	$0 \sim 0.15$	$\cdots$
$f_0(1500)$	0	$-0.33 \sim 0.18$	$0.28 \sim 0.79$	0	$-0.15 \sim -0.088$	$0.044 \sim 0.16$

lation in scenario 1, the asymptotic form of twist-3 LCDAs is used.

III. $B \to S$ FORM FACTORS AND SEMILEPTONIC DECAYS IN THE PQCD APPROACH

A. A brief review of pQCD approach

The basic idea of pQCD approach is including the intrinsic transverse momenta of valence quarks in the calculation of the hadronic matrix elements. The transition matrix element (see Fig. 1) of B meson to a scalar meson ($q_1\bar{q}_2$ component is supposed) can be expressed as the convolution of the wave functions Φ_B, Φ_S and the hard scattering kernel T_H, integrated over the longitudinal and transverse momenta of the valence quarks:

$$\mathcal{M} \propto \int_0^1 dx_1 dx_2 \int_{-\infty}^{\infty} \frac{d^2\vec{k}_{1\perp}}{(2\pi)^2} \frac{d^2\vec{k}_{2\perp}}{(2\pi)^2} \Phi_B(x_1, \vec{k}_{1\perp}, p_B, t) \times T_H(x_1, x_2, \vec{k}_{1\perp}, \vec{k}_{2\perp}, t)\Phi_S(x_2, \vec{k}_{2\perp}, p_1, t). \quad (17)$$

It is convenient to calculate the transition amplitude in coordinate space. Through the Fourier transformation, the above equation becomes

$$\mathcal{M} \propto \int_0^1 dx_1 dx_2 \int_{-\infty}^{\infty} d^2\vec{b}_1 d^2\vec{b}_2 \Phi_B(x_1, \vec{b}_1, p_B, t) \times T_H(x_1, x_2, \vec{b}_1, \vec{b}_2, t)\Phi_S(x_2, \vec{b}_2, p_1, t). \quad (18)$$

In principle, loop corrections to scattering kernel T_H can be taken into consideration, which usually bring two types of infrared divergences in individual diagrams: soft and collinear. Soft divergence is generated when all the components of a loop momentum l go to zero:

$$l^\mu = (l^+, l^-, \vec{l}_T) = (\Lambda, \Lambda, \vec{\Lambda}), \quad (19)$$

with l^μ expressed in the light-cone coordinate. The collinear divergence arises from the region where the gluon momentum is parallel to the massless quark momentum:

$$l^\mu = (l^+, l^-, \vec{l}_T) = (m_B, \Lambda^2/m_B, \vec{\Lambda}). \quad (20)$$

In both cases, the loop integration corresponds to $\int d^4l/l^4 \sim \log\Lambda$, thus logarithmic divergences are generated. In perturbation theory, it has been shown order by order that these divergences can be separated from the hard kernel and absorbed into meson wave functions using eikonal approximation [13]. When the soft and collinear momenta overlap, one also encounters double logarithm divergences, which can be resummed into the Sudakov factor and its expression is given in the Appendix.

The loop corrections to the weak decay vertex will generate another type of double logarithm. For example, the amplitude of the left diagram of Fig. 1 is proportional to $1/(x_2^2 x_1)$. When $x_2 \to 0$, additional collinear divergences are associated with the internal quark. The integration of the amplitude will produce double logarithm $\alpha_s \ln^2 x_2$, and the resummation of this type of double logarithm gives rise to Sudakov factor $S_t(x_2)$ [14], which is usually called jet function. The similar jet function $S_t(x_1)$ is generated after the resummation of the same type of double logarithm of the right diagram in Fig. 1. The jet function decreases faster than any power of x as $x \to 0$, thus it kills the endpoint singularity effectively. The jet function has been parametrized in a form which is independent of the decay channels, twists, and flavors [15].

With the Sudakov factors included, the factorization formula of the form factor matrix element in pQCD approach is given by

$$\mathcal{M} \propto \int_0^1 dx_1 dx_2 \int_{-\infty}^{\infty} d^2\vec{b}_1 d^2\vec{b}_2 \Phi_B(x_1, \vec{b}_1, p_B, t) \times T_H(x_1, x_2, \vec{b}_1, \vec{b}_2, t)\Phi_S(x_2, \vec{b}_2, p_1, t) \times S_t(x_i)\exp[-S_B(t) - S_2(t)]. \quad (21)$$

B. Form factors in the pQCD approach

The form factors for $B_{(s)} \to S$ transition are defined by

$$\kappa_S\langle S(P_S)|\bar{q}\gamma_\mu\gamma_5 b|\bar{B}_{(s)}(P_{B_{(s)}})\rangle = -i\left\{\left[(P_{B_{(s)}} + P_S)_\mu - \frac{m^2_{B_{(s)}} - m^2_S}{q^2} q_\mu\right]F_1(q^2) + \frac{m^2_{B_{(s)}} - m^2_S}{q^2} q_\mu F_0(q^2)\right\}, \quad (22)$$

$$\kappa_S\langle S(P_S)|\bar{q}\sigma_{\mu\nu} b|\bar{B}_{(s)}(P_{B_{(s)}})\rangle = -i\epsilon_{\mu\nu\alpha\beta} p_1^\alpha q^\beta \frac{2F_T(q^2)}{m_{B_{(s)}} + m_S}, \quad (23)$$

$$\kappa_S\langle S(P_S)|\bar{q}\sigma_{\mu\nu}\gamma_5 b|\bar{B}_{(s)}(P_{B_{(s)}})\rangle = [q_\mu P_{S\nu} - P_{S\mu} q_\nu]\frac{2F_T(q^2)}{m_{B_{(s)}} + m_S}, \quad (24)$$

with $q = P_{B_{(s)}} - P_S$. κ_S is the flavor factor for the transi-

tion: $\sqrt{2}$ for the component of $\bar{u}u$ in the $\frac{\bar{u}u \pm \bar{d}d}{\sqrt{2}}$ state, $\pm\sqrt{2}$ for the component of $\bar{d}d$ in the $\frac{\bar{u}u \pm \bar{d}d}{\sqrt{2}}$ state, 1 for the other states. In the large-recoil region, a hard gluon is required to kick the soft spectator antiquark to a fast-moving antiquark. Therefore, in this kinematics region, the form factors can be calculated perturbatively. The lowest order diagrams for the $B_{(s)} \to S$ transition are shown in Fig. 1. Carrying out the calculation under pQCD approach, we obtain the analytic formulas of the form factors nearby the $q^2 = 0$:

$$\begin{aligned} F_0(\eta) = 8\pi C_F m_B^2 \int_0^1 dx_1 dx_2 \int_0^\infty b_1 db_1 b_2 db_2 \phi_B(x_1, b_1)\{[\eta(x_2\eta - \eta - 1)\phi_S(x_2) - r_2\eta(2x_2 - 1)\phi_S^T(x_2) \\ + r_2(2x_2\eta - 3\eta + 2)\phi_S^s(x_2)]h_e(x_1, (1 - x_2)\eta, b_1, b_2)\alpha_s(t_e^1)\exp[-S_{ab}(t_e^1)]S_t(x_2) \\ + 2r_2\eta\phi_S^s(x_2)h_e(1 - x_2, x_1\eta, b_2, b_1)\alpha_s(t_e^2)\exp[-S_{ab}(t_e^2)]S_t(x_1)\}, \end{aligned} \tag{25}$$

$$\begin{aligned} F_1(\eta) = 8\pi C_F m_B^2 \int_0^1 dx_1 dx_2 \int_0^\infty b_1 db_1 b_2 db_2 \phi_B(x_1, b_1)\{[(x_2\eta - \eta - 1)\phi_S(x_2) + r_2(-2x_2 + 3 - 2/\eta)\phi_S^T(x_2) \\ - r_2(1 - 2x_2)\phi_S^s(x_2)]h_e(x_1, (1 - x_2)\eta, b_1, b_2)\alpha_s(t_e^1)\exp[-S_{ab}(t_e^1)]S_t(x_2) \\ + 2r_2\phi_S^s(x_2)h_e(1 - x_2, x_1\eta, b_2, b_1)\alpha_s(t_e^2)\exp[-S_{ab}(t_e^2)]S_t(x_1)\}, \end{aligned} \tag{26}$$

$$\begin{aligned} F_T(\eta) = 8\pi C_F m_B^2(1 + r_2) \int_0^1 dx_1 dx_2 \int_0^\infty b_1 db_1 b_2 db_2 \phi_B(x_1, b_1)\{[r_2(x_2 - 1)\phi_S^s(x_2) - \phi_S(x_2) \\ + r_2(x_2 - 1 - 2/\eta)\phi_S^T(x_2)]h_e(x_1, (1 - x_2)\eta, b_1, b_2)\alpha_s(t_e^1)\exp[-S_{ab}(t_e^1)]S_t(x_2) \\ + 2r_2\phi_S^s(x_2)h_e(1 - x_2, x_1\eta, b_2, b_1)\alpha_s(t_e^2)\exp[-S_{ab}(t_e^2)]S_t(x_1)\}. \end{aligned} \tag{27}$$

With these formulas we calculate the form factors nearby $q^2 = 0$. Through fitting the results among the region $0 < q^2 < 10\ \mathrm{GeV}^2$, we extrapolate them with the pole model parametrization

$$F_i(q^2) = \frac{F_i(0)}{1 - a(q^2/m_B^2) + b(q^2/m_B^2)^2}, \tag{28}$$

where a, b are the constants to be determined from the fitting procedure.

C. Semileptonic $B_{(s)}$ meson decays

The effective Hamiltonian for $b \to u l \bar{\nu}_l$ transition is

$$\mathcal{H}_{\mathrm{eff}}(b \to u l \bar{\nu}_l) = \frac{G_F}{\sqrt{2}} V_{ub}\bar{u}\gamma_\mu(1 - \gamma_5)b\bar{l}\gamma^\mu(1 - \gamma_5)\nu_l. \tag{29}$$

With the Hamiltonian, the q^2 dependant decay width $\frac{d\Gamma}{dq^2}$ can be expressed as

$$\begin{aligned} \frac{d\Gamma}{dq^2} = \frac{G_F^2|V_{ub}|^2}{192\pi^3 m_B^3}\frac{q^2 - m_l^2}{(q^2)^2} \\ \times \sqrt{\frac{(q^2 - m_l^2)^2}{q^2}}\sqrt{\frac{(m_B^2 - m_S^2 - q^2)^2}{4q^2} - m_S^2} \\ \times [(m_l^2 + 2q^2)(q^2 - (m_B - m_S)^2) \\ \times (q^2 - (m_B + m_S)^2)F_1^2(q^2) \\ + 3m_l^2(m_B^2 - m_S^2)^2 F_0^2(q^2)], \end{aligned} \tag{30}$$

with m_l as the mass of the lepton.

The calculation of $b \to s l^+ l^-$ transition is a bit complicated, because both the short-distance and long-distance contribution should be taken into consideration. The weak effective Hamiltonian is

$$\mathcal{H}_{\mathrm{eff}} = -\frac{G_F}{\sqrt{2}} V_{tb}V_{ts}^* \sum_{i=1}^{10} C_i(\mu)O_i(\mu), \tag{31}$$

with the doubly Cabibbo-Kobayashi-Maskawa suppressed terms omitted. $C_i(\mu)$ are the Wilson coefficients and the local operators $O_i(\mu)$ are given by [16]

$$
\begin{aligned}
O_1 &= (\bar{s}_\alpha c_\alpha)_{V-A}(\bar{c}_\beta b_\beta)_{V-A},\\
O_2 &= (\bar{s}_\alpha c_\beta)_{V-A}(\bar{c}_\beta b_\alpha)_{V-A},\\
O_3 &= (\bar{s}_\alpha b_\alpha)_{V-A}\sum_q(\bar{q}_\beta q_\beta)_{V-A},\\
O_4 &= (\bar{s}_\alpha b_\beta)_{V-A}\sum_q(\bar{q}_\beta q_\alpha)_{V-A},\\
O_5 &= (\bar{s}_\alpha b_\alpha)_{V-A}\sum_q(\bar{q}_\beta q_\beta)_{V+A},\\
O_6 &= (\bar{s}_\alpha b_\beta)_{V-A}\sum_q(\bar{q}_\beta q_\alpha)_{V+A},\\
O_7 &= \frac{em_b}{8\pi^2}\bar{s}\sigma^{\mu\nu}(1+\gamma_5)bF_{\mu\nu},\\
O_9 &= \frac{\alpha_{\rm em}}{8\pi}(\bar{l}\gamma_\mu l)(\bar{s}\gamma^\mu(1-\gamma_5)b),\\
O_{10} &= \frac{\alpha_{\rm em}}{8\pi}(\bar{l}\gamma_\mu\gamma_5 l)(\bar{s}\gamma^\mu(1-\gamma_5)b),
\end{aligned}
\tag{32}
$$

where $(\bar{q}_1q_2)_{V-A}(\bar{q}_3q_4)_{V-A} \equiv (\bar{q}_1\gamma^\mu(1-\gamma_5)q_2)\times(\bar{q}_3\gamma_\mu(1-\gamma)q_4)$, and $(\bar{q}_1q_2)_{V-A}(\bar{q}_3q_4)_{V+A} \equiv (\bar{q}_1\gamma^\mu(1-\gamma_5)q_2)(\bar{q}_3\gamma_\mu(1+\gamma)q_4)$. In Eq. (32), the term suppressed by m_s in O_7 is neglected.

The amplitude for $b\to sl^+l^-$ transition can be decomposed as

$$
\begin{aligned}
\mathcal{A}(b\to sl^+l^-) = \frac{G_F}{2\sqrt{2}}\frac{\alpha_{\rm em}}{\pi}V_{ts}^*V_{tb}\Big\{&C_9^{\rm eff}(\mu)[\bar{s}\gamma_\mu(1-\gamma_5)b]\\
&\times[\bar{l}\gamma^\mu l]+C_{10}[\bar{s}\gamma_\mu(1-\gamma_5)b][\bar{l}\gamma^\mu\gamma_5 l]\\
&-2m_bC_7^{\rm eff}(\mu)\Big[\bar{s}i\sigma_{\mu\nu}\frac{q^\nu}{q^2}(1+\gamma_5)b[\bar{l}\gamma^\mu l]\Big]\Big\},
\end{aligned}
\tag{33}
$$

where $\hat{s}=q^2/m_B^2$ and $\hat{m}_b=m_b/m_B$, with m_b as the b quark mass in the $\overline{\rm MS}$ scheme. The long-distance and short-distance contributions are absorbed into the $C_7^{\rm eff}(\mu)$ and $C_9^{\rm eff}(\mu)$, with

TABLE IV. The values of Wilson coefficients $C_i(m_b)$ in the leading logarithmic approximation in the standard model, with $m_W = 80.4$ GeV, $m_t = 173.8$ GeV, $m_b = 4.8$ GeV [18].

C_1	C_2	C_3	C_4	C_5	C_6	C_7	C_9	C_{10}
1.119	−0.270	0.013	−0.027	0.009	−0.033	−0.322	4.344	−4.669

$$
\begin{aligned}
C_7^{\rm eff}(\mu) &= C_7(\mu) + C'_{b\to s\gamma}(\mu),\\
C_9^{\rm eff}(\mu) &= C_9(\mu) + Y_{\rm pert}(\hat{s}) + Y_{\rm LD}(\hat{s}).
\end{aligned}
\tag{34}
$$

$Y_{\rm pert}$ represents the perturbative contributions, and $Y_{\rm LD}$ is the long-distance part. The $Y_{\rm pert}$ is given by [17]

$$
\begin{aligned}
Y_{\rm pert}(\hat{s}) = h(\hat{m}_c,\hat{s})C_0 &- \tfrac{1}{2}h(1,\hat{s})(4C_3+4C_4+3C_5+C_6)\\
&- \tfrac{1}{2}h(0,\hat{s})(C_3+3C_4)\\
&+ \tfrac{2}{9}(3C_3+C_4+3C_5+C_6),
\end{aligned}
\tag{35}
$$

with $C_0 = C_1+3C_2+3C_3+C_4+3C_5+C_6$. The Wilson coefficients, listed in Table IV, are given in the leading logarithmic accuracy. The long-distance part $Y_{\rm LD}$, involving the contributions of $B_{(s)}\to SV(c\bar{c})$ resonances where $V(c\bar{c})$ are the charmonium states, is neglected in this paper because of the lack of the experimental data. The corrections of the nonfactorizable effects of the charm quark loop to the $b\to s\gamma$ transition at $q^2=0$ are also neglected. And the absorptive part of $b\to s\gamma$ with neglecting the small contribution from $V_{tb}V_{ts}^*$ is represented by the $C'_{b\to s\gamma}$ part in $C_7^{\rm eff}$, which is given by [for a complete expression of $C_7^{\rm eff}(\mu)$, see [19]]

$$
C'_{b\to s\gamma}(\mu) = i\alpha_s[\tfrac{2}{9}\eta^{14/23}(G_I(x_t)-0.1687)-0.03C_2(\mu)],
\tag{36}
$$

with $G_I(x_t) = \frac{x_t(x_t^2-5x_t-2)}{8(x_t-1)^3}+\frac{3x_t^2\ln^2 x_t}{4(x_t-1)^4}$, $\eta=\alpha_s(m_W)/\alpha_s(\mu)$ and $x_t = m_t^2/m_W^2$.

The q^2 dependant width of $B\to Sl^+l^-$ is given by

$$
\begin{aligned}
\frac{d\Gamma}{dq^2} = \frac{G_F^2\alpha_{\rm em}^2|V_{tb}|^2|V_{ts}^*|^2\sqrt{\lambda}}{1024m_B^3\pi^5}\sqrt{\frac{q^2-4m_l^2}{q^2}}\Big[&\frac{4}{3}\lambda\Big|\frac{C_9^{\rm eff}}{2}F_1(q^2)+\frac{C_{10}}{2}F_1(q^2)\sqrt{\frac{q^2-4m_l^2}{q^2}}+C_7^{\rm eff}\frac{m_bF_T(q^2)}{m_B+m_S}\Big|^2\\
&+\frac{4}{3}\lambda\Big|\frac{C_9^{\rm eff}}{2}F_1(q^2)-\frac{C_{10}}{2}F_1(q^2)\sqrt{\frac{q^2-4m_l^2}{q^2}}+C_7^{\rm eff}\frac{m_bF_T(q^2)}{m_B+m_S}\Big|^2+\frac{4\lambda}{3q^2}\Big|C_9^{\rm eff}m_lF_1(q^2)+C_7^{\rm eff}\frac{2m_l^2m_bF_T(q^2)}{m_B+m_S}\Big|^2\\
&+4|m_lC_{10}(m_B^2-m_S^2)F_0(q^2)|^2\Big],
\end{aligned}
\tag{37}
$$

with $\lambda=(m_B^2-q^2-m_S^2)^2-4m_S^2q^2$.

IV. NUMERICAL RESULTS AND DISCUSSION

A. Form factors

Our results of the $B\to S$ form factors are listed in Table V and VI. The errors for the form factors in those two tables arise from the uncertainties of hadronic parameters of $B_{(s)}$ meson (f_B and ω_b), $\Lambda_{\rm QCD}$ (0.20 GeV–0.30 GeV), factorization scales [see Eqs. (A1)], and the Gegenbauer moments of scalar mesons. A number of remarks will be given in order.

(i) Compared with transitions of B meson to pseudoscalar mesons, vector mesons, and axial-vector me-

TABLE V. Form factors for $B \to S$ in scenario 1. The errors arise from the uncertainties of hadronic parameters of $B_{(s)}$ meson (f_b and ω_b), $\Lambda_{\rm QCD}$, scales (t_e^i), and the Gegenbauer moments of scalar mesons.

	$F_0(0) = F_1(0)$	$F_T(0)$	$a(F_0)$	$b(F_0)$	$a(F_1)$	$b(F_1)$	$a(F_T)$	$b(F_T)$
$B \to \sigma$	$0.28^{+0.07}_{-0.06}$	$0.29^{+0.07}_{-0.06}$	$0.65^{+0.01}_{-0.07}$	$-0.11^{+0.00}_{-0.13}$	$1.61^{+0.04}_{-0.06}$	$0.56^{+0.04}_{-0.10}$	$1.67^{+0.05}_{-0.05}$	$0.62^{+0.06}_{-0.06}$
$B \to a_0(980)$	$0.39^{+0.10}_{-0.08}$	$0.45^{+0.11}_{-0.10}$	$0.72^{+0.08}_{-0.03}$	$-0.16^{+0.12}_{-0.00}$	$1.68^{+0.03}_{-0.06}$	$0.62^{+0.01}_{-0.10}$	$1.70^{+0.06}_{-0.03}$	$0.63^{+0.11}_{-0.01}$
$B \to \kappa(800)$	$0.27^{+0.07}_{-0.06}$	$0.29^{+0.07}_{-0.07}$	$0.71^{+0.04}_{-0.08}$	$-0.12^{+0.02}_{-0.12}$	$1.65^{+0.06}_{-0.04}$	$0.59^{+0.08}_{-0.04}$	$1.69^{+0.06}_{-0.05}$	$0.65^{+0.08}_{-0.06}$
$B \to f_0(1370)$	$-0.30^{+0.08}_{-0.09}$	$-0.39^{+0.10}_{-0.11}$	$0.70^{+0.07}_{-0.02}$	$-0.24^{+0.15}_{-0.05}$	$1.63^{+0.09}_{-0.05}$	$0.53^{+0.14}_{-0.08}$	$1.60^{+0.06}_{-0.04}$	$0.50^{+0.08}_{-0.05}$
$B \to a_0(1450)$	$-0.31^{+0.08}_{-0.09}$	$-0.41^{+0.10}_{-0.12}$	$0.70^{+0.13}_{-0.02}$	$-0.26^{+0.24}_{-0.00}$	$1.63^{+0.08}_{-0.04}$	$0.53^{+0.13}_{-0.06}$	$1.62^{+0.04}_{-0.07}$	$0.54^{+0.03}_{-0.13}$
$B \to K_0^*(1430)$	$-0.34^{+0.07}_{-0.09}$	$-0.44^{+0.10}_{-0.11}$	$0.72^{+0.04}_{-0.04}$	$-0.18^{+0.04}_{-0.05}$	$1.65^{+0.04}_{-0.07}$	$0.57^{+0.08}_{-0.14}$	$1.61^{+0.04}_{-0.05}$	$0.52^{+0.05}_{-0.06}$
$\bar{B}_s^0 \to f_0(980)$	$0.35^{+0.09}_{-0.07}$	$0.40^{+0.10}_{-0.08}$	$0.73^{+0.04}_{-0.06}$	$-0.13^{+0.02}_{-0.09}$	$1.66^{+0.06}_{-0.05}$	$0.60^{+0.07}_{-0.05}$	$1.70^{+0.06}_{-0.04}$	$0.66^{+0.06}_{-0.05}$
$\bar{B}_s^0 \to \kappa(800)$	$0.29^{+0.07}_{-0.06}$	$0.31^{+0.07}_{-0.06}$	$0.66^{+0.07}_{-0.03}$	$-0.17^{+0.11}_{-0.00}$	$1.62^{+0.03}_{-0.05}$	$0.56^{+0.00}_{-0.09}$	$1.68^{+0.05}_{-0.03}$	$0.62^{+0.10}_{-0.01}$
$\bar{B}_s^0 \to f_0(1500)$	$-0.26^{+0.09}_{-0.08}$	$-0.34^{+0.10}_{-0.10}$	$0.72^{+0.14}_{-0.08}$	$-0.20^{+0.10}_{-0.10}$	$1.61^{+0.13}_{-0.03}$	$0.48^{+0.27}_{-0.02}$	$1.60^{+0.06}_{-0.04}$	$0.48^{+0.09}_{-0.04}$
$\bar{B}_s^0 \to K_0^*(1430)$	$-0.32^{+0.06}_{-0.07}$	$-0.41^{+0.08}_{-0.09}$	$0.69^{+0.05}_{-0.03}$	$-0.21^{+0.11}_{-0.03}$	$1.62^{+0.06}_{-0.03}$	$0.52^{+0.14}_{-0.04}$	$1.62^{+0.01}_{-0.06}$	$0.56^{+0.00}_{-0.16}$

sons [8,20], our predictions on $B \to S$ form factors in scenario 2 are obviously larger, which is caused mainly by the large decay constants ($\bar{f}_S$) of the scalar mesons. For example, the form factor $F_0(0)$ of the B meson to pion transition is about 0.23 [9] with 0.131 GeV as the decay constant of pion, while the B meson to $a_0(980)$ transition in scenario 1 has 0.39 as its corresponding form factor, whose decay constant is more than 2 times larger than pion.

(ii) In Table V, the form factors of $B \to \sigma$ are smaller than those of $B \to a_0(980)$. Because the same decay constant and Gegenbauer moments for these two particles are used in the calculation, the differences are caused by the mass differences between $a_0(980)$ and σ (0.98 GeV for $a_0(980)$ and 0.513 GeV for σ [1]). In scenario 1, there are small differences between $\kappa(800)$ and $f_0(600)$ in masses [0.672 GeV for $\kappa(800)$], decay constants, and Gegenbauer moments. Besides, the contribution from twist-2 LCDA of $\kappa(800)$, which is proportional to f_S, is too small to give sizable differences. Thus the $B \to \sigma$ and $B \to \kappa(800)$ have nearly the same form factors as shown in Table V. Comparing the form factors of $B \to \kappa(800)$ with $\bar{B}_s^0 \to \kappa(800)$ in Table V, one can find that the differences between B and $\bar{B}_s^0$ mesons affect little. Therefore, the large differences between the form factors of $\bar{B}_s^0 \to \kappa(800)$ and those of $B \to a_0(980)$ are mainly due to the large difference between the scalar meson masses.

(iii) The form factors of B to heavier nonet transition in scenario 1 are negative, while the others are positive. The reason is that the decay constants ($\bar{f}_S$) of the heavier nonet in scenario 1 have opposite signs to the others, which is clearly shown in Tables I and II.

(iv) As we can see from Tables V and VI, the predictions in scenario 2 are larger than the corresponding ones in scenario 1 roughly by a factor of 2 in magnitude. In order to show how these large differences are generated, we take the form factor $F_0(0)$ as an example and list contributions from different terms in LCDAs in Table VII. (Data is given with asymptotic forms of twist-3 LCDAs are adopted in both scenario 1 and scenario 2, because the terms with Gegenbauer moments bring so small effects, which is discussed in the following, that they cannot change the argument.) The contributions from the two twist-3 LCDAs ϕ_S^s and ϕ_S^T are given in the first two columns. The numbers in the column "B_1" denotes the contributions from the Gegenbauer moments B_1 in twist-2 LCDAs. It is also similar for the fourth B_3 column. The last column collects the total contributions to the form factors. The different inputs between scenario 1 and in scenario 2 are the decay constants and Gegenbauer moments. If only twist-3 LCDAs are taken into account, the form factors will be proportional to the decay constant. Since the decay constants $\bar{f}_S$ in $S2$ are (typically 60%) larger than those in $S1$ in magnitude, the form factors are

TABLE VI. Form factors for $B \to S$ in scenario 2, with the same error sources as the data in Table V.

	$F_0(0) = F_1(0)$	$F_T(0)$	$a(F_0)$	$b(F_0)$	$a(F_1)$	$b(F_1)$	$a(F_T)$	$b(F_T)$
$B \to f_0(1370)$	$0.63^{+0.23}_{-0.14}$	$0.76^{+0.37}_{-0.17}$	$0.70^{+0.05}_{-0.11}$	$-0.14^{+0.02}_{-0.09}$	$1.60^{+0.15}_{-0.05}$	$0.53^{+0.18}_{-0.09}$	$1.63^{+0.07}_{-0.05}$	$0.57^{+0.07}_{-0.07}$
$B \to a_0(1450)$	$0.68^{+0.19}_{-0.15}$	$0.92^{+0.30}_{-0.21}$	$0.62^{+0.05}_{-0.08}$	$-0.21^{+0.06}_{-0.02}$	$1.73^{+0.12}_{-0.07}$	$0.70^{+0.16}_{-0.11}$	$1.68^{+0.06}_{-0.04}$	$0.61^{+0.10}_{-0.02}$
$B \to K_0^*(1430)$	$0.60^{+0.18}_{-0.15}$	$0.78^{+0.25}_{-0.19}$	$0.68^{+0.07}_{-0.05}$	$-0.18^{+0.06}_{-0.01}$	$1.70^{+0.09}_{-0.07}$	$0.65^{+0.10}_{-0.10}$	$1.68^{+0.07}_{-0.04}$	$0.61^{+0.11}_{-0.02}$
$\bar{B}_s^0 \to f_0(1500)$	$0.60^{+0.20}_{-0.12}$	$0.82^{+0.30}_{-0.16}$	$0.65^{+0.04}_{-0.10}$	$-0.22^{+0.07}_{-0.02}$	$1.76^{+0.13}_{-0.08}$	$0.71^{+0.20}_{-0.08}$	$1.71^{+0.04}_{-0.07}$	$0.66^{+0.06}_{-0.10}$
$\bar{B}_s^0 \to K_0^*(1430)$	$0.56^{+0.16}_{-0.13}$	$0.72^{+0.22}_{-0.17}$	$0.67^{+0.06}_{-0.07}$	$-0.17^{+0.01}_{-0.07}$	$1.69^{+0.08}_{-0.07}$	$0.63^{+0.09}_{-0.10}$	$1.68^{+0.06}_{-0.06}$	$0.63^{+0.07}_{-0.08}$

TABLE VII. Contributions from different LCDAs to the $B \to S$ form factor F_0 in scenario 1 ($S1$) or scenario 2 ($S2$). The contributions from the two twist-3 LCDAs ϕ_S^s and ϕ_S^T are given in the first two columns. The numbers in the column "B_1" denote the contributions from the Gegenbauer moments B_1 in twist-2 LCDAs. It is also similar for the fourth column. The last column collects the total contributions to the form factors (data is given with asymptotic forms of twist-3 LCDAs adopted in both scenario 1 and scenario 2).

		ϕ_S^s	ϕ_S^T	B_1	B_3	Total
$B \to a_0(1450)$	$S1$:	-0.21	-0.05	0.14	-0.19	-0.31
	$S2$:	0.35	0.08	0.15	0.11	0.69
$B \to K_0^*(1430)$	$S1$:	-0.22	-0.05	0.10	-0.18	-0.34
	$S2$:	0.33	0.07	0.14	0.09	0.62
$\bar{B}_s^0 \to f_0(1500)$	$S1$:	-0.17	-0.04	0.11	-0.16	-0.26
	$S2$:	0.32	0.08	0.13	0.09	0.61
$\bar{B}_s^0 \to K_0^*(1430)$	$S1$:	-0.19	-0.05	0.09	-0.17	-0.32
	$S2$:	0.27	0.07	0.14	0.09	0.58

accordingly larger. The ϕ_S^s term give much larger contributions than the ϕ_S^T term. Contributions from the Gegenbauer moments of the twist-2 LCDAs sizably enhance the form factors in $S2$ but not too much in $S1$. For B to scalar meson transitions in scenario 1, the B_1 terms provide contributions with the same sign with the twist-3 terms, while the terms with B_3 have the opposite sign. Thus, the two terms of the twist-2 LCDAs give destructive contributions to the total form factors in $S1$. The situation is different in $S2$; although the two Gegenbauer moments are small in magnitude, they give constructive contributions and induce much larger form factors.

(v) We also investigate the contributions from terms with Gegenbauer moments in twist-3 LCDAs, and find that the effects brought by these moments are not large. Taking $B \to f_0(1370)$ transition as an example, a comparison between the cases with and without these contributions is given in Table VIII. We can see that most of the results are changed by less than 10%.

(vi) Compared with our previous study on $B \to f_0$, $K_0^*(1430)$ transitions [21,22], the predictions for the form factors given in the present work are a bit smaller. The main reason is that different values for the threshold resummation parameters c have been used. Moreover, the form factors in this paper are larger than those obtained in other approaches or models [23–26]. As a result, the branching ratios of the semileptonic decays are larger, which is discussed in the following.

As we have mentioned in the Introduction section, the experimentalists have already provided many investigations on nonleptonic B decays involving a scalar meson in the final state. Among these decays, the so-called color-allowed tree-dominated processes can be directly utilized to estimate the $B \to S$ form factors, under the hypothesis of factorization. For example, the $\bar{B}^0 \to a_0^+ \pi^-$ decay amplitude in the factorization scheme is expressed as

$$\begin{aligned}\mathcal{A}(\bar{B}^0 \to a_0^+ \pi^-) = \frac{G_F}{\sqrt{2}} m_B^2 f_\pi F_0^{B\to a_0}\{V_{ub}V_{ud}^*[a_1 + a_4 \\ + a_{10} - r_\pi(a_6 + a_8)] \\ + V_{cb}V_{cd}^*[a_4 + a_{10} - r_\pi(a_6 + a_8)]\},\end{aligned} \tag{38}$$

where a_i is the combination of Wilson coefficient

$$\begin{aligned} a_1 &= C_2 + C_1/3, \qquad a_2 = C_1 + C_2/3, \\ a_i &= C_i + C_{i+1}/N_c \quad (i = 3, 5, 7, 9), \\ a_i &= C_i + C_{i-1}/N_c \quad (i = 4, 6, 8, 10). \end{aligned} \tag{39}$$

$a_1 \sim 1$, and it has small uncertainties. Although there are large uncertainties for a_3–a_{10}, the combination of Wilson coefficients satisfies:

$$a_1 \gg \max[a_{3-10}]. \tag{40}$$

If only the branching ratios are concerned, contributions from the penguin operators (a_{3-10} terms) can be safely neglected and thus

$$\mathcal{A}(\bar{B}^0 \to a_0^+ \pi^-) = \frac{G_F}{\sqrt{2}} m_B^2 f_\pi F_0^{B\to a_0} V_{ub}V_{ud}^* a_1. \tag{41}$$

If the partial decay widths are well determined experimentally, these results will directly constrain the B to scalar meson transition form factors. The upper bounds for $B \to a_0\pi$ are given as (in units of 10^{-6})

$$\begin{aligned} \mathcal{B}\mathcal{R}(B \to a_0^\pm(980)\pi^\mp) < 3.1, \\ \mathcal{B}\mathcal{R}(B \to a_0^\pm(1450)\pi^\mp) < 2.3, \end{aligned} \tag{42}$$

where the daughter branching fraction has taken to be 100%. Since the scalar mesons $a_0(980)$ and $a_0(1450)$ have vanishing decay constants in the isospin limit, the

TABLE VIII. Form factors for $B \to f_0(1370)$. The first line and the second line are the results with and without contributions from the terms with Gegenbauer moments in twist-3 LCDAs, respectively.

$F_0(0) = F_1(0)$	$F_T(0)$	$a(F_0)$	$b(F_0)$	$a(F_1)$	$b(F_1)$	$a(F_T)$	$b(F_T)$
$0.63^{+0.23}_{-0.14}$	$0.76^{+0.37}_{-0.17}$	$0.70^{+0.05}_{-0.11}$	$-0.14^{+0.02}_{-0.09}$	$1.60^{+0.15}_{-0.05}$	$0.53^{+0.18}_{-0.09}$	$1.63^{+0.07}_{-0.05}$	$0.57^{+0.07}_{-0.07}$
$0.67^{+0.17}_{-0.14}$	$0.83^{+0.21}_{-0.18}$	$0.71^{+0.02}_{-0.07}$	$-0.12^{+0.00}_{-0.11}$	$1.64^{+0.04}_{-0.05}$	$0.57^{+0.04}_{-0.07}$	$1.65^{+0.05}_{-0.04}$	$0.59^{+0.07}_{-0.03}$

branching ratios of $\bar{B}^0 \to a_0^- \pi^+$ are very small and one expects the relation: $\mathcal{BR}(B \to a_0^{\pm} \pi^{\mp}) = \mathcal{BR}(\bar{B}^0 \to a_0^+ \pi^-)$. Compared with the branching ratio of $\bar{B}^0 \to \pi^+ \pi^-$ (in units of 10^{-6}),

$$\mathcal{B}\,\mathcal{R}(B \to \pi^+ \pi^-) = 5.16 \pm 0.22, \tag{43}$$

results provide the upper bound for the $B \to a_0$ form factors:

$$\begin{aligned} F_0(B \to a_0(980)) &< 0.78 F_0(B \to \pi) = 0.18, \\ F_0(B \to a_0(1450)) &< 0.67 F_0(B \to \pi) = 0.15, \end{aligned} \tag{44}$$

where as a rough estimation, we have taken $F_0(B \to \pi) = 0.23$ [9]. Compared with our results in Tables V and VI, one

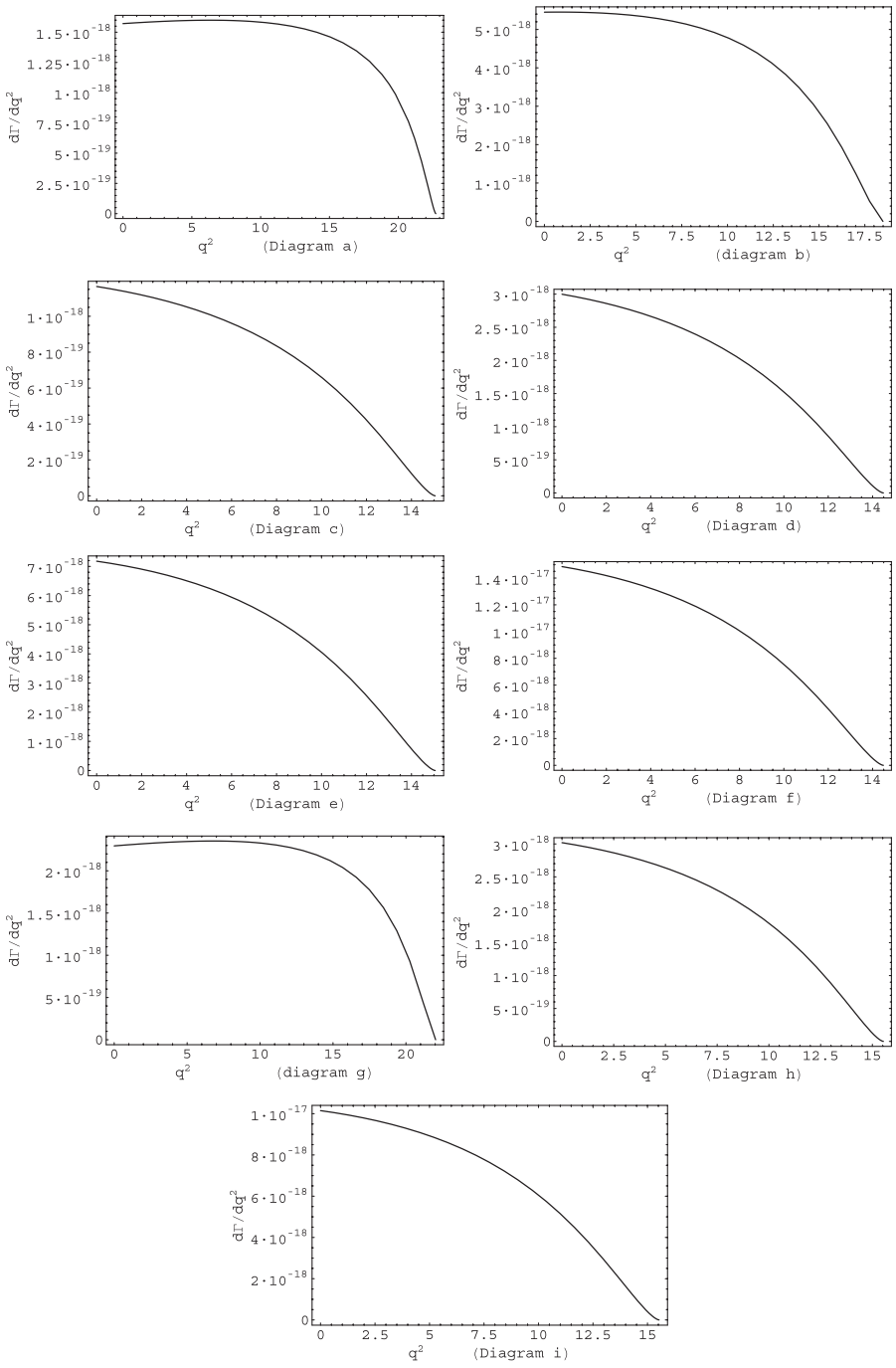

FIG. 2. Partial decay widths of the semileptonic $B \to Sl\bar{\nu}$ decays as functions of q^2. Diagrams a–d denote the $B^- \to (\sigma, a_0^+(980), f_0(1370), a_0^+(1450)) l^- \bar{\nu}_l$ in scenario 1, respectively; diagrams e–f denote the $B^- \to (f_0(1370), a_0^+(1450)) l^- \bar{\nu}_l$ in scenario 2, respectively; diagram g: $\bar{B}_s \to \kappa^+(800) l^- \bar{\nu}_l$ in scenario 1; diagram h: $\bar{B}_s \to K_0^{*+}(1430) l^- \bar{\nu}_l$ in scenario 1; diagram i: $\bar{B}_s \to K_0^{*+}(1430) l^- \bar{\nu}_l$ in scenario 2.

can see our results have exceeded the present experimental upper bound. Despite that, it does not mean our predictions are ruled out by the data, as the daughter decay is not taken into account in the derivation for the experimental bound. Our predictions will be confronted with the real bound in the future, whenever the daughter decay of a_0 is well studied.

B. Decay widths and branching fractions

With the form factors at hand, one can directly obtain the partial decay width through Eqs. (30) and (37). Since masses of electrons and muons are very small compared with q^2 in the most kinematic region of the semileptonic decays, they will not produce large effects and are ne-

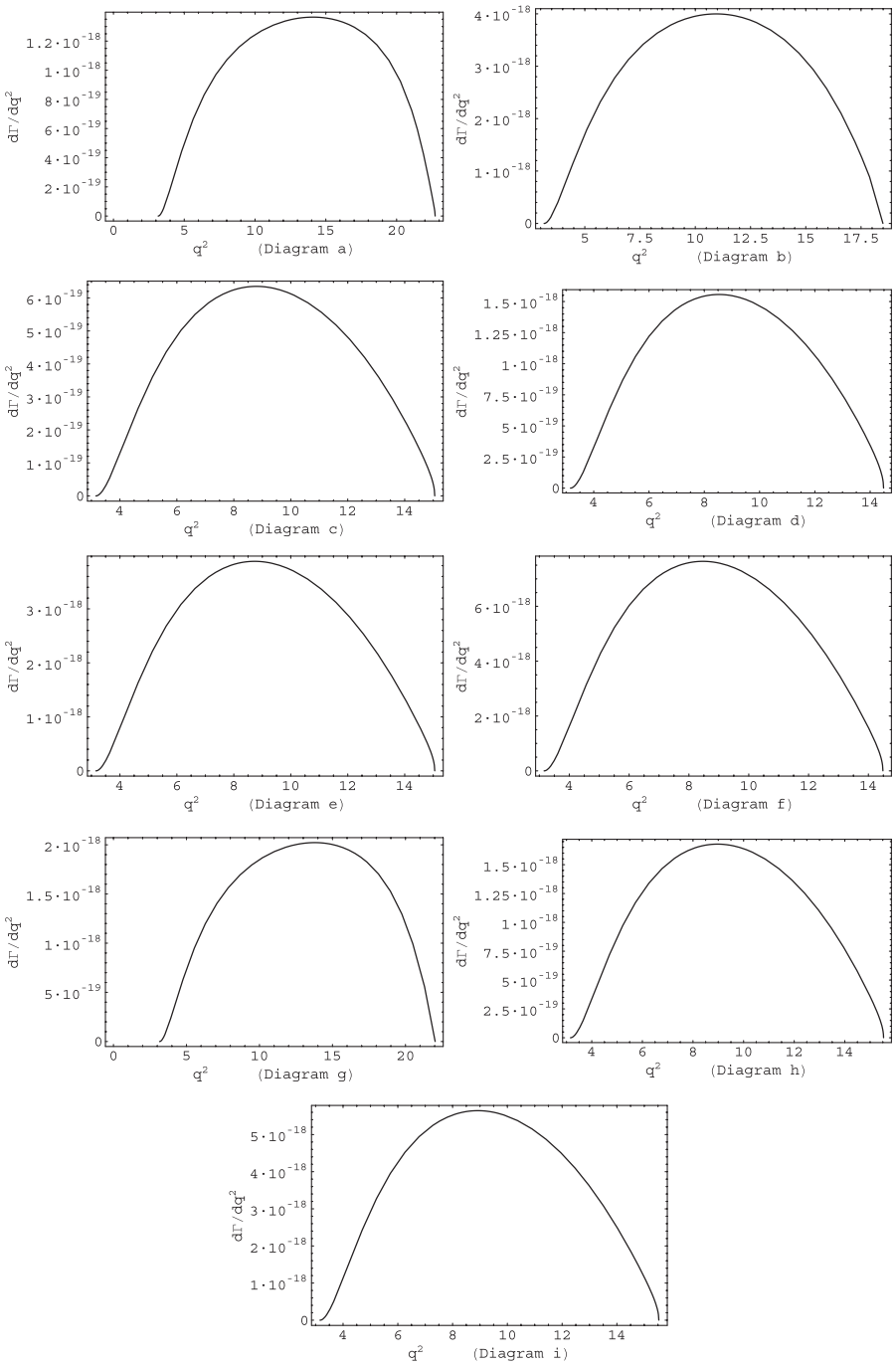

FIG. 3. Partial decay widths of the semileptonic $B \to S\tau\bar{\nu}$ decays as functions of q^2. Diagram a: $B^- \to \sigma\tau^-\bar{\nu}_l$ in scenario 1; diagram b: $\bar{B}^0 \to a_0^+(980)\tau^-\bar{\nu}_l$ in scenario 1; diagram c: $B^- \to f_0(1370)\tau^-\bar{\nu}_l$ in scenario 1; diagram d: $\bar{B}^0 \to a_0^+(1450)\tau^-\bar{\nu}_l$ in scenario 1; diagram e: $B^- \to f_0(1370)\tau^-\bar{\nu}_l$ in scenario 2; diagram f: $\bar{B}^0 \to a_0^+(1450)\tau^-\bar{\nu}_l$ in scenario 2; diagram g: $\bar{B}_s \to \kappa^+(800)\tau^-\bar{\nu}_l$ in scenario 1; diagram h: $\bar{B}_s \to K_0^{*+}(1430)\tau^-\bar{\nu}_l$ in scenario 1; diagram i: $\bar{B}_s \to K_0^{*+}(1430)\tau^-\bar{\nu}_l$ in scenario 2.

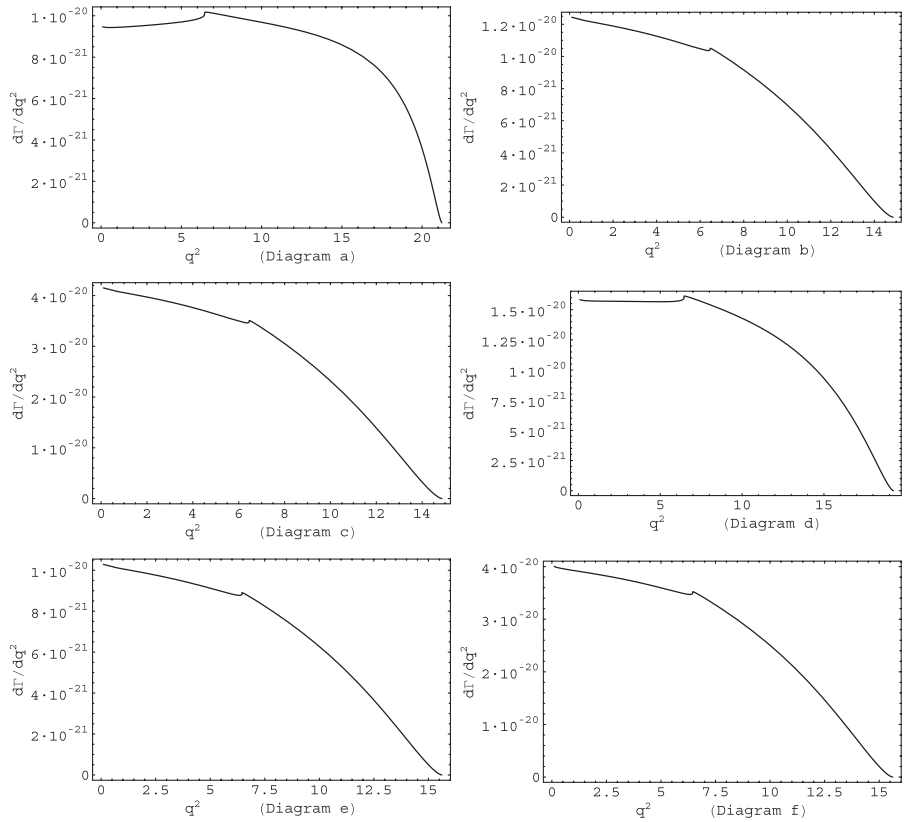

FIG. 4. Partial decay widths of the semileptonic $B \to Sl^+l^-(l = e, \mu)$ decays as functions of q^2. Diagram a: $B^- \to \kappa^- l^+ l^-$ in scenario 1; diagram b: $B^- \to K_0^{*-}(1430) l^+ l^-$ in scenario 1; diagram c: $B^- \to K_0^{*-}(1430) \times l^+ l^-$ in scenario 2; diagram d: $\bar{B}_s^0 \to f_0(980) l^+ l^-$ in scenario 1; diagram e: $\bar{B}_s^0 \to f_0(1500) l^+ l^-$ in scenario 1; diagram f: $\bar{B}_s^0 \to f_0(1500) l^+ l^-$ in scenario 2.

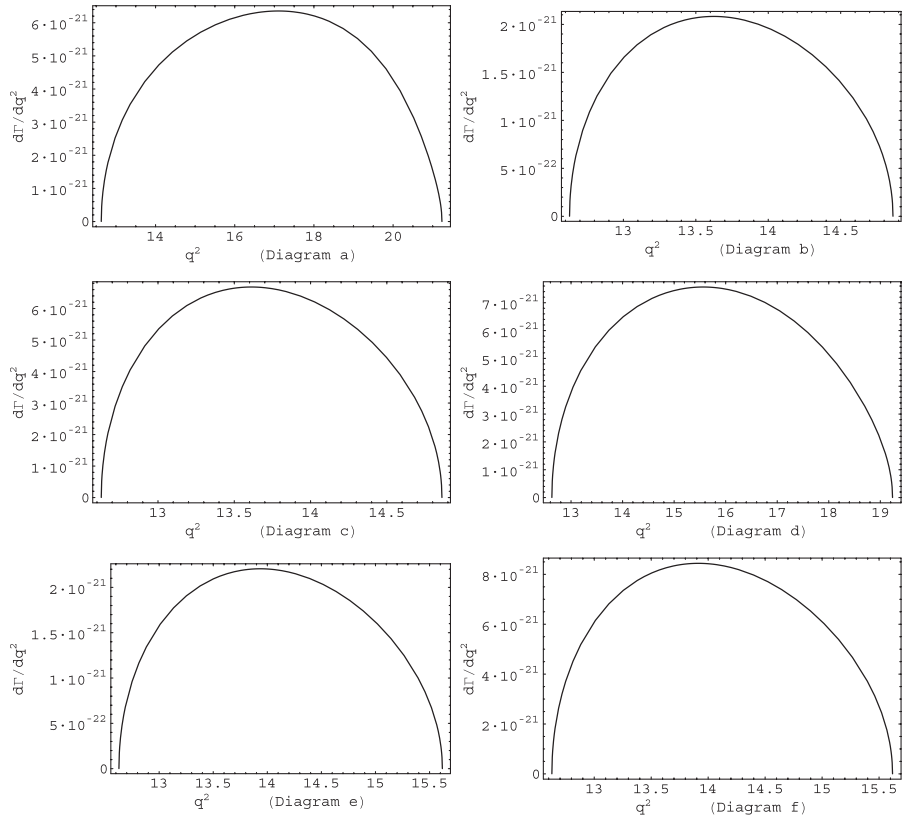

FIG. 5. Partial decay widths of the semileptonic $B \to S\tau^+\tau^-$ decays as functions of q^2. Diagram a: $B^- \to \kappa^- \tau^+ \tau^-$ in scenario 1; diagram b: $B^- \to K_0^{*-}(1430) \tau^+ \tau^-$ in scenario 1; diagram c: $B^- \to K_0^{*-}(1430) \times \tau^+ \tau^-$ in scenario 2; diagram d: $\bar{B}_s^0 \to f_0(980) \tau^+ \tau^-$ in scenario 1; diagram e: $\bar{B}_s^0 \to f_0(1500) \times \tau^+ \tau^-$ in scenario 1; diagram f: $\bar{B}_s^0 \to f_0(1500) \tau^+ \tau^-$ in scenario 2.

TABLE IX. The total branching ratios for the $b \to u l \bar{\nu}_l$ in scenario 1 (unit: 10^{-4}). The errors are estimated with errors from the form factors.

	$B \to S e \bar{\nu}_e (\mu \bar{\nu}_\mu)$	$B \to S \tau \bar{\nu}_\tau$
$B^- \to \sigma$	$0.81^{+0.52}_{-0.31}$	$0.51^{+0.33}_{-0.19}$
$\bar{B}^0 \to a_0^+(980)$	$1.84^{+1.09}_{-0.73}$	$1.01^{+0.61}_{-0.40}$
$B^- \to f_0(1370)$	$0.29^{+0.19}_{-0.13}$	$0.13^{+0.09}_{-0.06}$
$\bar{B}^0 \to a_0^+(1450)$	$0.67^{+0.41}_{-0.29}$	$0.28^{+0.17}_{-0.12}$
$\bar{B}_s \to \kappa^+(800)$	$1.42^{+0.82}_{-0.53}$	$0.88^{+0.52}_{-0.33}$
$\bar{B}_s \to K_0^{*+}(1430)$	$0.77^{+0.37}_{-0.27}$	$0.35^{+0.17}_{-0.12}$

TABLE X. Same as Table IX except in scenario 2.

	$B^- \to f_0(1370) e \bar{\nu}_e (\mu \bar{\nu}_\mu)$	$B^- \to f_0(1370) \tau \bar{\nu}_\tau$
This work	$1.55^{+1.53}_{-0.65}$	$0.67^{+0.68}_{-0.29}$
	$\bar{B}^0 \to a_0^+(1450) e \bar{\nu}_e (\mu \bar{\nu}_\mu)$	$\bar{B}^0 \to a_0^+(1450) \tau \bar{\nu}_\tau$
This work	$3.25^{+2.36}_{-1.36}$	$1.32^{+0.97}_{-0.57}$
LCSR [23]	$1.8^{+0.9}_{-0.7}$	$0.63^{+0.34}_{-0.25}$
	$\bar{B}_s \to K_0^{*+}(1430) e \bar{\nu}_e (\mu \bar{\nu}_\mu)$	$\bar{B}_s \to K_0^{*+}(1430) \tau \bar{\nu}_\tau$
This work	$2.45^{+1.77}_{-1.05}$	$1.09^{+0.82}_{-0.47}$
LCSR [23]	$1.3^{+1.3}_{-0.4}$	$0.52^{+0.57}_{-0.18}$
QCDSR [24]	$0.36^{+0.38}_{-0.24}$	

glected in this work. In Figs. 2 and 3, we give our predictions on the partial decay width of $B_{(s)} \to S l^- \bar{\nu}_l$ ($l = e, \mu$) and $B_{(s)} \to S \tau^- \bar{\nu}_l$, respectively. The diagrams in Figs. 4 and 5 are similar but for the $B_{(s)} \to S l^+ l^-$ ($l = e, \mu$) and $B_{(s)} \to S \tau^+ \tau^-$ decays. In Fig. 4, there exists a small discontinuity in each diagram, which is caused by the discontinuities in functions $h(\hat{m}_c, \hat{s})$ and $h(1, \hat{s})$ in Eq. (35). When $l = \tau$ in Fig. 5, the discontinuities in the diagrams disappear, because the origins of q^2 axes become $4m_\tau^2$ which is large enough to ensure that the variation of q^2 does not pass the discontinuities in the $h(\hat{m}_c, \hat{s})$ and $h(1, \hat{s})$ functions.

TABLE XI. The total branching ratios for the $b \to s l^+ l^-$ in scenario 1 (unit:10^{-7}) with the same error sources as Tables IX and X.

	$B \to S e^+ e^- (\mu^+ \mu^-)$	$B \to S \tau^+ \tau^-$
$B^- \to \kappa^-$	$4.38^{+2.73}_{-1.84}$	$0.56^{+0.36}_{-0.25}$
$B^- \to K_0^{*-}(1430)$	$3.13^{+1.73}_{-1.21}$	$2.00^{+1.16}_{-0.77} \times 10^{-2}$
$\bar{B}_s^0 \to f_0^0(980)$	$5.21^{+3.23}_{-2.06}$	$0.38^{+0.25}_{-0.16}$
$\bar{B}_s^0 \to f_0^0(1500)$	$1.74^{+1.14}_{-0.94}$	$2.21^{+1.32}_{-1.21} \times 10^{-2}$

The results for the total branching ratios are collected in Tables IX, X, XI, and XII, with the errors estimated with the errors of the form factors. One can find that the branching ratios with τ lepton(s) in the final state are smaller than the ones without τ lepton(s), because the large mass of τ lepton(s) makes the phase space much smaller. In Table IX, $\frac{Br(B_{(s)} \to S e \bar{\nu}_e)}{Br(B_{(s)} \to S \tau \bar{\nu}_\tau)}$ is smaller than 2 when the scalar meson belongs to the light nonet. While for the heavy nonet mesons, the value of this ratio is larger than 2. The reason is that more energy is released when the final state is a light meson, and thus the effect of m_τ on the phase space is not so evident. In Tables X and XII, we also list the predictions in light-cone sum rules (LCSR) and QCD sum rules (QCDSR), which are smaller than our predictions. The reason is that we have bigger form factors. Taking $\bar{B}^0 \to a_0^+(1450) e^- \bar{\nu}_e$ as an example, the form factors that contribute are $F_0(q^2)$ and $F_1(q^2)$, with the relationship $F_0(0) = F_1(0)$. $F_0(0)$ for $\bar{B}^0 \to a_0^+(1450)$ in scenario 2 in this paper is $0.68^{+0.19}_{-0.15}$, while the corresponding value in [23] is 0.52 ± 0.10. As a rough estimation, supposing that corresponding form factors in these two papers have analogical evolution with respect to q^2, the branching ratio in this paper should be $(0.69/0.52)^2 \approx 1.7$ times larger.

V. CONCLUSIONS

In this work, we have studied the $B \to S$ form factors in the pQCD approach under two different scenarios for the scalar mesons. In scenario 1, both of the light and heavy nonet are described as the $\bar{q}q$ state while in scenario 2, we have only studied the heavy nonet. Because of the large decay constant $\bar{f}_S$, we have found that most of our predictions are larger than those for the $B \to P$ transition form factors, especially in scenario 2. Contributions from various LCDAs are explicitly specified. Because of the large

TABLE XII. Same as Table IX except in scenario 2.

	$B^- \to K_0^{*-}(1430) e^+ e^- (\mu^+ \mu^-)$	$B^- \to K_0^{*-}(1430) \tau^+ \tau^-$
This work	$9.78^{+7.66}_{-4.40}$	$6.29^{+5.71}_{-2.95} \times 10^{-2}$
LCSR [23]	$5.7^{+3.4}_{-2.4}$	$9.8^{+12.4}_{-5.5} \times 10^{-2}$
Light front quark model [25]	1.63	2.86×10^{-2}
QCDSR [26]	$2.09 - 2.68$	$(1.70 - 2.20) \times 10^{-2}$
	$\bar{B}_s^0 \to f_0^0(1500) e^+ e^- (\mu^+ \mu^-)$	$\bar{B}_s^0 \to f_0^0(1500) \tau^+ \tau^-$
This work	$10.0^{+8.5}_{-3.8}$	$0.13^{+0.12}_{-0.06}$
LCSR [23]	$5.3^{+2.3}_{-1.8}$	$0.12^{+0.08}_{-0.05}$

masses of $a_0(1450)$, $K_0^*(1430)$, $f_0(1500)$, their twist-3 LCDAs have provided more than one-half contributions to the form factors in both scenarios. In scenario 1, the two Gegenbauer moments B_1, B_3 for the twist-2 LCDAs have different signs and they give destructive contributions to the form factors; while in scenario 2, although the two Gegenbauer moments are small in magnitudes, they give constructive contributions and induce larger form factors. Contributions from terms with Gegenbauer moments in the twist-3 LCDAs are also investigated, and we find that these terms do not give large changes. We also study the semileptonic $B \to Sl\bar{\nu}$ and $B \to Sl^+l^-$ decays, including the partial decay width and the integrated branching fractions. Branching ratios of the semileptonic $B \to Sl\bar{\nu}$ decays are found to have the order of 10^{-4}, while branching fractions of the $B \to Sl^+l^-$ decays have the order of 10^{-7}. Compared with results in the previous studies, our predictions are a bit larger which is caused by larger form factors. These predictions will be tested by the future experiments.

ACKNOWLEDGMENTS

This work is partly supported by the National Natural Science Foundation of China under Grants No. 10735080, No. 10625525, No. 10525523, and No. 10805037. This research is also supported in part by the Project of Knowledge Innovation Program (PKIP) of Chinese Academy of Sciences, Grant No. KJCX2.YW.W10.

APPENDIX: PQCD FUNCTIONS

In this part, we collect the functions which are essential in the pQCD calculation:

$$t_e^1 = \max(t_c\sqrt{(1-x_2)\eta}m_B, 1/b_1, 1/b_2),$$
$$t_e^2 = \max(t_c\sqrt{x_1\eta}m_B, 1/b_1, 1/b_2), \tag{A1}$$

with $t_c = 1$ for the calculation of the central values and $t_c = 0.75$–1.25 for error estimation:

$$\begin{aligned} h_e(x_1, x_2, b_1, b_2) = {} & K_0(\sqrt{x_1x_2}m_Bb_1)[\theta(b_1-b_2) \\ & \times K_0(\sqrt{x_2}m_Bb_1)I_0(\sqrt{x_2}m_Bb_2) \\ & + \theta(b_2-b_1)K_0(\sqrt{x_2}m_Bb_2) \\ & \times I_0(\sqrt{x_2}m_Bb_1)]. \end{aligned} \tag{A2}$$

$$S_t(x) = \frac{2^{1+2c}\Gamma(3/2+c)}{\sqrt{\pi}\Gamma(1+c)}[x(1-x)]^c, \tag{A3}$$

with $c = 0.4$. The Sudakov factor in Eqs. (25)–(27) is given by

$$S_{ab}(t) = S_B(t) + S_S(t), \tag{A4}$$

where

$$S_B(t) = s\left(x_1\frac{m_B}{\sqrt{2}}, b_1\right) + \frac{5}{3}\int_{1/b_1}^{t}\frac{d\bar{\mu}}{\bar{\mu}}\gamma_q(\alpha_s(\bar{\mu})), \tag{A5}$$

$$\begin{aligned} S_S(t) = {} & s\left(x_2\frac{m_B}{\sqrt{2}}, b_2\right) + s\left((1-x_2)\frac{m_B}{\sqrt{2}}, b_2\right) \\ & + 2\int_{1/b_2}^{t}\frac{d\bar{\mu}}{\bar{\mu}}\gamma_q(\alpha_s(\bar{\mu})), \end{aligned} \tag{A6}$$

with the quark anomalous dimension $\gamma_q = -\alpha_s/\pi$. The explicit form for the function $s(Q, b)$ is

$$\begin{aligned} s(Q,b) = {} & \frac{A^{(1)}}{2\beta_1}\hat{q}\ln\left(\frac{\hat{q}}{\hat{b}}\right) - \frac{A^{(1)}}{2\beta_1}(\hat{q}-\hat{b}) + \frac{A^{(2)}}{4\beta_1^2}\left(\frac{\hat{q}}{\hat{b}}-1\right) \\ & - \left[\frac{A^{(2)}}{4\beta_1^2} - \frac{A^{(1)}}{4\beta_1}\ln\left(\frac{e^{2\gamma_E-1}}{2}\right)\right]\ln\left(\frac{\hat{q}}{\hat{b}}\right) \\ & + \frac{A^{(1)}\beta_2}{4\beta_1^3}\hat{q}\left[\frac{\ln(2\hat{q})+1}{\hat{q}} - \frac{\ln(2\hat{b})+1}{\hat{b}}\right] \\ & + \frac{A^{(1)}\beta_2}{8\beta_1^3}[\ln^2(2\hat{q}) - \ln^2(2\hat{b})], \end{aligned} \tag{A7}$$

where the variables are defined by

$$\hat{q} \equiv \ln[Q/(\sqrt{2}\Lambda)], \qquad \hat{b} \equiv \ln[1/(b\Lambda)], \tag{A8}$$

and the coefficients $A^{(i)}$ and β_i are

$$\begin{aligned} \beta_1 &= \frac{33-2n_f}{12}, \qquad \beta_2 = \frac{153-19n_f}{24}, \\ A^{(1)} &= \frac{4}{3}, \qquad A^{(2)} = \frac{67}{9} - \frac{\pi^2}{3} - \frac{10}{27}n_f + \frac{8}{3}\beta_1\ln\left(\frac{1}{2}e^{\gamma_E}\right), \end{aligned} \tag{A9}$$

n_f is the number of the quark flavors, and γ_E is the Euler constant. We will use the one-loop running coupling constant, i.e. we pick up only the four terms in the first line of the expression for the function $s(Q, b)$.

[1] C. Amsler *et al.* (Particle Data Group), Phys. Lett. B **667**, 1 (2008).

[2] S. Godfrey and J. Napolitano, Rev. Mod. Phys. **71**, 1411 (1999).

[3] F. E. Close and N. A. Törnqvist, J. Phys. G **28**, R249 (2002).
[4] A. Garmash *et al.* (Belle Collaboration), Phys. Rev. D **65**, 092005 (2002).
[5] E. Barberio *et al.* (Heavy Flavor Averaging Group), arXiv:0808.1297. The updated results can be found at www.slact.stanford.edu/xorg/hfag.
[6] Y. Y. Keum, H.-n. Li, and A. I. Sanda, Phys. Rev. D **63**, 054008 (2001); Phys. Lett. B **504**, 6 (2001); C. D. Lü, K. Ukai, and M. Z. Yang, Phys. Rev. D **63**, 074009 (2001).
[7] A. G. Grozin and M. Neubert, Phys. Rev. D **55**, 272 (1997); M. Beneke and T. Feldmann, Nucl. Phys. **B592**, 3 (2001); M. Beneke, G. Buchalla, M. Neubert, and C. T. Sachrajda, Nucl. Phys. **B591**, 313 (2000).
[8] C. D. Lu and M. Z. Yang, Eur. Phys. J. C **28**, 515 (2003).
[9] A. Ali, G. Kramer, Y. Li, C. D. Lu, Y. L. Shen, W. Wang, and Y. M. Wang, Phys. Rev. D **76**, 074018 (2007).
[10] H. Y. Cheng, C. K. Chua, and K. C. Yang, Phys. Rev. D **73**, 014017 (2006).
[11] M. Alford and R. L. Jaffe, Nucl. Phys. **B578**, 367 (2000); H. Y. Cheng, Phys. Rev. D **67**, 034024 (2003); A. V. Anisovich, V. V. Anisovich, and V. A. Nikonov, Eur. Phys. J. A **12**, 103 (2001); Phys. At. Nucl. **65**, 497 (2002); A. Gokalp, Y. Sarac, and O. Yilmaz, Phys. Lett. B **609**, 291 (2005).
[12] C. D. Lu, Y. M. Wang, and H. Zou, Phys. Rev. D **75**, 056001 (2007).
[13] H.-n. Li and H. L. Yu, Phys. Rev. D **53**, 2480 (1996).
[14] H.-n. Li, Phys. Rev. D **66**, 094010 (2002).
[15] H.-n. Li and K. Ukai, Phys. Lett. B **555**, 197 (2003).
[16] A. J. Buras, M. Misiak, M. Munz, and S. Pokorski, Nucl. Phys. **B424**, 374 (1994).
[17] A. J. Buras and M. Munz, Phys. Rev. D **52**, 186 (1995).
[18] H. Hatanaka and K. C. Yang, Phys. Rev. D **78**, 074007 (2008).
[19] C. H. Chen and C. Q. Geng, Phys. Rev. D **64**, 074001 (2001).
[20] W. Wang, R. H. Li, and C. D. Lu, arXiv:0711.0432.
[21] W. Wang, Y. L. Shen, Y. Li, and C. D. Lu, Phys. Rev. D **74**, 114010 (2006).
[22] Y. L. Shen, W. Wang, J. Zhu, and C. D. Lu, Eur. Phys. J. C **50**, 877 (2007).
[23] Y. M. Wang, M. J. Aslam, and C. D. Lu, Phys. Rev. D **78**, 014006 (2008).
[24] M. Z. Yang, Phys. Rev. D **73**, 034027 (2006); **73**, 079901 (E) (2006).
[25] C. H. Chen, C. Q. Geng, C. C. Lih, and C. C. Liu, Phys. Rev. D **75**, 074010 (2007).
[26] T. M. Aliev, K. Azizi, and M. Savei, Phys. Rev. D **76**, 074017 (2007).